Adenine Protonation in Domain B of the Hairpin Ribozyme[†]

Sapna Ravindranathan, Samuel E. Butcher, and Juli Feigon*

Department of Chemistry and Biochemistry, 405 Hilgard Avenue, University of California, Los Angeles, California 90095-1569

Received August 21, 2000; Revised Manuscript Received October 26, 2000

ABSTRACT: Protein enzymes often use ionizable side chains, such as histidine, for general acid−base catalysis because the imidazole pK_a is near neutral pH. RNA enzymes, on the other hand, are comprised of nucleotides which do not have apparent pK_a values near neutral pH. Nevertheless, it has been recently shown that cytidine and adenine protonation can play an important role in both nucleic acid structure and catalysis. We have employed heteronuclear NMR methods to determine the pK_a values and time scales of chemical exchanges associated with adenine protonation within the catalytically essential B domain of the hairpin ribozyme. The large, adenine-rich internal loop of the B domain allows us to determine adenine pK_a values for a variety of non-Watson−Crick base pairs. We find that adenines within the internal loop have pK_a values ranging from 4.8 to 5.8, significantly higher than the free mononucleotide pK_a of 3.5. Adenine protonation results in potential charge stabilization, hydrogen bond formation, and stacking interactions that are expected to stabilize the internal loop structure at low pH. Fast proton exchange times of 10−50 μs were determined for the well-resolved adenines. These results suggest that shifted pK_a values may be a common feature of adenines in non-Watson−Crick base pairs, and identify two adenines which may participate in hairpin ribozyme active site chemistry.

The most effective acid−base catalysts at neutral pH have pK_a values near 7, thus accounting for the widespread use of histidines in protein enzyme active sites (*1*). RNA enzymes (ribozymes) are also capable of general acid−base catalysis, though the closest pK_a values to neutral pH of free nucleotide monophosphates are quite low (CMP = 4.2, AMP = 3.5) (*2*). Unique structural environments can shift these pK_as toward neutral pH, allowing the formation of protonated bases and thereby expanding both the structural and enzymatic properties of nucleic acids. However, little information exists regarding how non-Watson−Crick base pairing in RNA can alter these apparent pK_a values. Shifted adenine pK_as have been observed to stabilize A^+•C base pairs near neutral pH (*3*, *4*). Recently, a protonated adenine has been proposed to catalyze peptidyl transfer within the active site of the ribosome (*5*, *6*). Additionally, a protonated cytidine acts as a general acid in the catalytic mechanism of the hepatitis delta virus ribozyme (*7*). In DNA, protonated adenines have been observed to form salt bridges (*8*, *9*), and cytidine protonation stabilizes triple helix formation (*10*) and C-tetraplexes (*11*).

Naturally occurring self-cleaving RNAs include the hairpin, hammerhead, hepatitis delta, and VS ribozymes (*12*). All of these ribozymes catalyze site-specific phosphoryl transfer reactions, producing cleavage products with 2′,3′-cyclic phosphates and 5′-OH groups. However, these ribozymes are both structurally and mechanistically different. For example, the hammerhead and hepatitis delta virus ribozymes utilize a metal ion-bound hydroxy anion in their active site as a general base (*7*, *12*). The hairpin ribozyme, on the other hand, has a metal ion-independent mechanism, and efficiently functions with cobalt hexamine, an inert metal complex (*13*). It therefore seems plausible that the hairpin ribozyme may employ a protonated base as a general acid, in a manner similar to the hepatitis delta virus ribozyme. Such a mechanism would also be consistent with reaction kinetics which indicate a pK_a of 5.4 (*13*).

The hairpin ribozyme is composed of two domains, A and B (Figure 1), which interact in the transition state. Domain A contains the substrate strand and forms a duplex containing a small internal loop. The NMR structure of this domain has been determined by Cai et al. (*4*). We recently solved the structure of the catalytically essential B domain of the hairpin ribozyme by NMR (*14*, *15*). The B domain contains a 16 nucleotide adenine-rich internal loop (Figure 1) that forms an underwound helix with an expanded minor groove, containing 7 non-Watson−Crick base pairs, including a nonprotonated A•C pair, 2 G•A pairs, a single hydrogen bond A•U reverse Hoogsteen pair, and 2 different types of A•A pairings (Figure 2). Six out of the eight adenines in the B domain internal loop are catalytically essential (*16*). In contrast, there is only one catalytically essential cytosine in the entire hairpin riboyzme, and this cytosine is believed to form a long-range Watson−Crick interaction between the A and B domains (*17*). Therefore, it is highly unlikely that cytosine protonation plays a role in hairpin ribozyme catalysis. The A domain contains two catalytically essential adenines (*16*). One of these adenines (A10) has a pK_a of 6.2, due to the formation of an A^+•C wobble pair that is also unlikely to be relevant to the transition state, since the observed interaction was with a nonessential cytosine derived from an HIV sequence (*4*). However, the internal loop of the B domain has many solvent-accessible adenine N1

[†] This work was supported by NSF and NIH grants to J.F.

* To whom correspondence should be addressed. Phone: (310) 206-6922. Fax: (310) 825-0982. E-mail: feigon@mbi.ucla.edu.

10.1021/bi001976r CCC: $19.00
Published on Web 11/30/2000

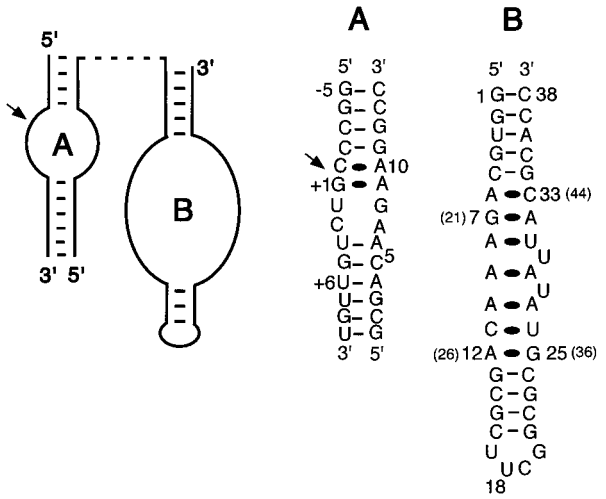

FIGURE 1: Schematic illustration of the hairpin ribozyme secondary structure, along with the sequence of the A and B domains used in the NMR structure determinations. The RNA cleavage site in domain A is marked with an arrow. A dashed line between the A and B domains represents a covalent connection in the intact ribozyme secondary structure. Non-Watson−Crick base pairings determined by NMR are indicated with ovals. The numbering system for the 38 nucleotide B domain used in these studies corresponds to the NMR construct, with the original hairpin ribozyme numbering scheme shown as adjacent numbers in parentheses. The B domain contains a stable helical extension and UUCG tetraloop not normally found in the ribozyme.

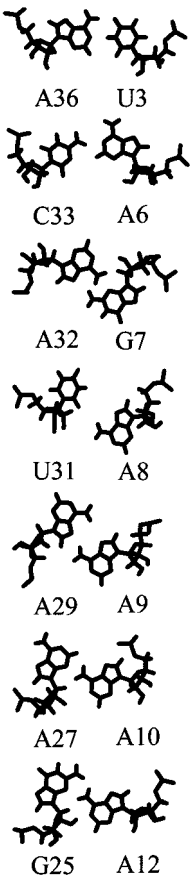

FIGURE 2: Orientations of the mismatched base pairs in the internal loop of the B domain of the hairpin ribozyme obtained from the solution NMR structure (*14*).

functional groups which could be positioned close to the substrate (*14*). We wished to determine if any of these functional groups possess shifted pK_a values that could participate in catalysis.

Legault and Pardi have shown that ^{13}C NMR is a powerful tool for studying adenine and cytidine protonation in RNA (*3*). Both the pK_a values and time scales of protonation can be measured, the former by fitting the Henderson−Hasselbach equation to the chemical shift changes as a function of pH and the latter by NMR line shape analysis. Here we use analysis of ^{1}H-^{13}C HSQC (*18*) spectra to study the protonation of the adenine N1 functional groups in the B domain of the hairpin ribozyme by monitoring the pH-induced changes in the chemical shifts and line widths of the C2 carbons. The adenine residues in the loop have a range of pK_a values from 4.8 to 5.8, significantly higher than the free mononucleotide pK_a value of 3.5. Analysis of the ^{13}C NMR line shapes shows that the chemical exchanges associated with adenine protonation occur on a very fast (microsecond) time scale in the loop as opposed to the millisecond time scale reported for imino proton exchange in Watson−Crick base pairs (*19*).

MATERIALS AND METHODS

Preparation of ^{13}C, ^{15}N-Labeled Hairpin Ribozyme B Domain Samples. ^{13}C,^{15}N-labeled B domain samples were prepared as previously described (*14*). Samples were 0.5 mM, 220 μL in a Shigemi NMR tube, in 50 mM NaCl, 90% H_2O/10% D_2O. The pHs of the samples were varied by adding 0.2 N HCl or 0.2 N NaOH to the desired pH value.

NMR Spectroscopy. The ^{1}H-^{13}C HSQC (*18*) spectra at different pHs (3.90, 4.00, 4.10, 4.40, 4.55, 5.30, 5.51, 5.82, 6.12, 6.60, 6.80, 7.60, and 8.40) were recorded on a Bruker DRX 500 MHz spectrometer. Spectra were obtained with 1024 points with a sweep width of 4045 Hz in t_2, and 256 points with a sweep width of 3019 Hz in the t_1 dimension. The proton carrier was set to 4.8 ppm, and the ^{13}C carrier was set to 145 ppm. All spectra were acquired at 303 K. For the line shape analysis, the line widths were measured from 1D slices of the 2D ^{1}H-^{13}C HSQC spectra Fourier-transformed without the use of any weighting function. Spectra used to determine the T_2 values were acquired as described (*20*).

Determination of Adenine pK_as. The pK_a values were determined by measuring changes in ^{13}C chemical shifts as a function of pH. The pK_a values were determined by nonlinear least-squares fit of experimental pH titration curves to the equation (*21*):

$$\delta_{obs} = [\delta_A + \delta_B \times 10^{(pH-pK_a)}]/[1 + 10^{(pH-pK_a)}] \quad (1)$$

δ_A and δ_B represent the chemical shifts corresponding to the protonated and unprotonated states, respectively (low and high extremes of pH). The above equation is derived from the Henderson−Hasselbach equation given by

$$pH = \log[(1 - p_A)/p_A] + pK_a \quad (2)$$

where p_A represents the fraction of protonated species. The observed chemical shift at a given pH is given by $\delta_{obs} = \delta_A p_A + \delta_B p_B$. The fraction of protonated species can be calculated as a ratio of the C2 chemical shift difference in the unprotonated state and a given pH (Δ) to the chemical shift difference between unprotonated and protonated states

(Δ_T). The Henderson−Hasselbach equation can now be written as

$$\mathrm{pH} = \log[(\Delta_T - \Delta)/\Delta] + \mathrm{p}K_a \quad (3)$$

If the chemical shifts of the protonated and unprotonated states can be determined from the experimental titration curves over the pH range investigated, then the pK_a values can be determined by linear regression analysis based on eq 3. In most cases, however, full experimental titration curves could not be obtained due to the severe overlap of signals at pH $\leq$4.0. In such cases, the experimental titration curves can be analyzed by fits to eq 1 with the chemical shifts at low pH (δ_A) and the pK_a treated as variables. For residues A6 and A32, the experimental titration curves are nearly complete, and clear transitions toward a low pH plateau are visible. The remaining residues also display a change in slope at low pH, and the corresponding apparent pK_a values can also be reasonably estimated due to the sigmoidal character of the curves and the presence of a steep inflection point at the pK_a. To evaluate the potential for error in the pK_a estimation, a test was done for residue A12, which does not display a clear low-pH plateau. Experimental data were included at pH 3.9, along with a nonexperimental extreme pH value of 3.0 and chemical shift plateau of 146 ppm. The resulting calculated apparent pK_a (5.02) was within the experimental error of the fit to eq 1 obtained using just the experimental data at pH 4.1 and above (5.1 $\pm$ 0.1).

Determination of Exchange Lifetimes. The lifetimes for exchange between protonated and unprotonated states were determined by analysis of the ^{13}C line shapes. The NMR signal line shape for a two-site (A and B) chemically exchanging system is derived from the modified Bloch equations and is given by (*22, 23*)

$$S(\nu) = [P(1 + \tau_{ex}(p_A/T_{2A} + p_B/T_{2B})) + QR]/(P^2 + R^2) \quad (4)$$

where $p_A + p_B = 1$, $\tau_{ex} = \tau_A\tau_B/(\tau_A + \tau_B)$, $P = \tau_{ex}[1/T_{2A}T_{2B} - (\pi(\nu_A + \nu_B) - 2\pi\nu)^2 + \pi^2(\nu_A - \nu_B)^2] + p_A/T_{2A} + p_B/T_{2B}$, $Q = \tau_{ex}[\pi(\nu_A + \nu_B) - 2\pi\nu - \pi(p_A - p_B)(\nu_A - \nu_B)]$, and $R = \pi(\nu_A - \nu_B)(p_A - p_B) - \tau_{ex}\pi(\nu_A - \nu_B)(1/T_{2A} - 1/T_{2B}) + [\pi(\nu_A + \nu_B) - 2\pi\nu][1 + \tau_{ex}(\nu_A + \nu_B)]$. τ_{ex} is the lifetime for exchange between protonated and unprotonated states, T_{2i} is the spin−spin relaxation time of state i, and ν_i is the frequency in state i, where i represents state A or B. The two-site exchange line shapes were simulated for different values of exchange times, and the rate of exchange and its error were determined by looking for the best fit between the experimental chemical shift and line widths at half-height to the calculated ones. The ^{13}C 1D spectra were extracted from the 2D spectra processed without the use of any weighting function, by selecting out slices parallel to the F_1 dimension. The chemical shifts and line widths were determined by fitting to a Lorentzian line shape using spectral deconvolution. The error in the exchange times was estimated from the error in the experimental line widths and the error in the chemical shift of the protonated state.

RESULTS

The secondary structure of the B domain RNA used in this study is shown in Figure 1. One of the nine adenines in the domain forms a Watson−Crick pair while the others are located within the internal loop and are exposed to solvent. ^{1}H-^{13}C HSQC spectra were obtained at different pH values, and the aromatic C2−H2 region of the spectrum was used to monitor N1 protonation. Figure 3 shows the C2−H2 region at three different pH values. All of the C2 resonances of the adenines in the internal loop shift downfield with increasing pH. The C2 resonance of A36, on the other hand, does not show any change in chemical shift as a function of pH. The A36 residue is the only Watson−Crick base-paired adenine in the B domain, and its N1 is therefore involved in a strong hydrogen bond. The pH-dependent changes in the chemical shifts were analyzed to determine the apparent pK_a values.

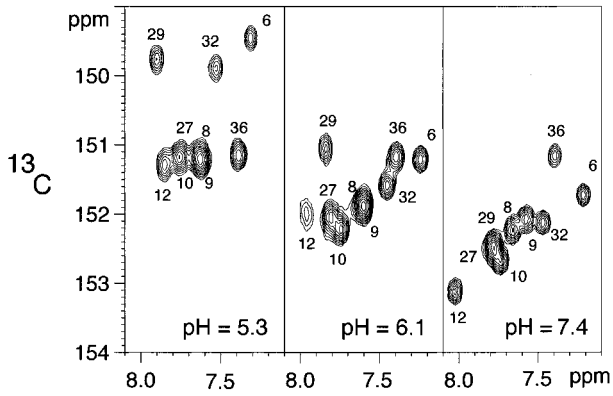

FIGURE 3: ^{1}H-^{13}C HSQC spectra of the B domain of the hairpin ribozyme showing the aromatic C2−H2 region at pH 5.3, 6.1, and 7.4. The cross-peaks are labeled with nucleotide number.

pH Titration Curves. Figure 4 shows the effect of pH on the chemical shifts of the C2 resonances of the adenine residues in the internal loop of B domain RNA. The pH titration curves (4.1−7.6) for all the adenine C2s in the internal loop have a sigmoidal dependence characteristic of a titration binding curve. In contrast, the Watson−Crick base-paired A36 shows no line width or chemical shift changes as a function of pH (plot not shown). The apparent pK_a values were determined from the fits of experimental data to eq 1, with the chemical shift at low pH (δ_A) and the pK_a as variables. The chemical shift at high pH (δ_B) was obtained from the experimental titration curves for all the adenine residues over the pH range examined. This corresponds to the chemical shift values observed at pH $\geq$7.6. Below pH 4.1, there is severe spectral overlap for all of the cross-peaks except A6 and A32, and therefore the additional data points acquired at pH 3.9 and 4.0 were not used in the curve fits. However, inclusion of these data points gives pK_as which are within the error limits of the values obtained without them. Furthermore, these data did indicate that the chemical shifts were approaching the plateau expected for the protonated state. The best fit curves and the estimated apparent pK_a values are indicated in Figure 4.

The values of δ_A obtained from the best fit of eq 1 to the experimental data for A6, A29, and A32 are close to the chemical shift values observed at pH 3.9. For these residues, the apparent pK_a values were also estimated by linear regression analysis based on eq 3. The total change in chemical shift, Δ_T, was determined from the difference in chemical shift values at pH 8.6 and 3.9. A6 and A32 have Δ_T values of 616 Hz, and A29 has a value of 636 Hz. The

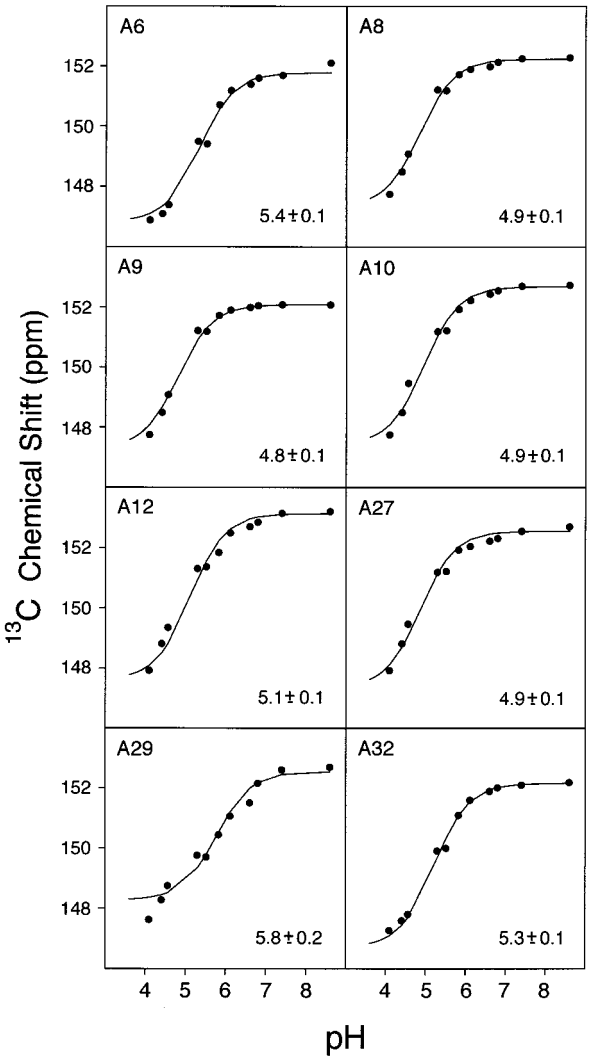

FIGURE 4: Plots of the chemical shifts versus pH of the C2 resonances of the adenine residues in non-Watson−Crick base pairs (A6, A8, A9, A10, A12, A27, A29, A32) in the B domain of the hairpin ribozyme. Solid lines are the best fit titration curves calculated based on eq 1. Values for the apparent pK_as determined for N1 protonation of the adenines are given on the figure.

value of Δ is obtained from the difference in chemical shift at pH 8.6 and the chemical shift value at any given pH. For A6 and A32, the apparent pK_a value obtained is 5.4 ± 0.1 with a slope of 0.93. For A29, the apparent pK_a value is 5.6 ± 0.1 with a slope 1.3. The slope obtained is close to 1 in all cases, as expected in the case of a single protonation event. All the adenine residues within the internal loop have higher apparent pK_a values compared to the value of 3.5 for the nucleotide monophosphate (Figure 4). A higher apparent pK_a value indicates that these bases can be readily protonated, and the NMR structure shows that the N1 sites of the adenines in the internal loop are solvent-accessible (Figure 5).

Exchange Lifetimes. Exchange processes occurring on the chemical shift time scale are reflected in the line shape of the signals from the nuclei which experience two or more electronic environments. The line shape depends on the fractional population of the two states, the spin−spin relaxation times of the nuclei in the two states, and the exchange times between the two states. The A6, A29, and A32 residues have sufficiently well-resolved C2 resonances for analysis. The fractional populations were determined as described above. The spin−spin (T_2) relaxation times determined for C2 functional groups in the protonated (pH 4.0) and unprotonated (pH ≥7.6) states are given in Table 1. The spin−spin relaxation time for C2 of A36 is the same within experimental error at both low and high pH. This shows that the overall relaxation behavior of the RNA does not change with pH. The residues A6, A29, and A32, on the other hand, have different T_2 values for the protonated and unprotonated states. Therefore, the observed changes in the C2 line widths within the internal loop are caused by the protonation equilibrium.

Table 1: C2 Spin−Spin Relaxation Times of A6, A32, A29, and A36

	T_2 (ms)	
residue	pH 4.0	pH 7.6
A6	14.6 ± 2	25.3 ± 1
A32	11.6 ± 3	27.0 ± 1
A29	20.4 ± 2	26.0 ± 2
A36	23.2 ± 1	24.1 ± 1

Table 2: C2 Line Widths and Time Scales of Chemical Exchanges Associated with Protonation of A6, A32, and A29 Residues in the B Domain

	A6		A32		A29	
pH	line width (Hz)	exchange time (μs)	line width (Hz)	exchange time (μs)	line width (Hz)	exchange time (μs)
4.4	35 ± 2	59 ± 9	39 ± 4	45 ± 11	28 ± 3	23 ± 5
4.55	38 ± 3	38 ± 6	43 ± 4	35 ± 9	30 ± 3	18 ± 4
5.3	35 ± 2	15 ± 2	42 ± 4	20 ± 4	45 ± 5	26 ± 4
5.51	29 ± 1	10 ± 1	37 ± 2	15 ± 2	40 ± 4	22 ± 4
5.82	26 ± 1	14 ± 2	35 ± 2	25 ± 3	42 ± 4	24 ± 3

The line widths (Table 2) and chemical shifts for the adenine C2s at different pH were determined from the 2D ^{1}H-^{13}C HSQC spectra. The lines are broader for the C2 resonances of A6, A29, and A32 at intermediate pH values compared to the line widths at extreme values of pH corresponding to the protonated (pH 4.0) and unprotonated (pH ≥7.6) states. On the other hand, the A36 C2 resonance shows no variation in line width as a function of pH, as expected for a base which forms a stable Watson−Crick pair.

The protonation kinetics for A6, A29, and A32 were studied by modeling the adenine C2s as a spin system undergoing two-site chemical exchange. The slope of 1 obtained from the Hill plot analysis of the protonation of the A6, A29, and A32 residues indicates a two-state model between the protonated and unprotonated forms and justifies the use of eq 4 for the determination of the exchange times associated with the protonation process. To determine the exchange time between the protonated and unprotonated states, the exchange line shape was simulated for different values of the exchange time using eq 4. The exchange times were determined from the best fit of the simulated line shapes to the experimental chemical shifts and line widths. The exchange times are of the order of 10−50 μs, indicating fast exchange (Table 2).

DISCUSSION

Role of Protonated Adenines. Raised adenine pK_a values have been previously observed for A^+·C wobble pairs in two different RNAs, the leadzyme (*3*) and domain A of the

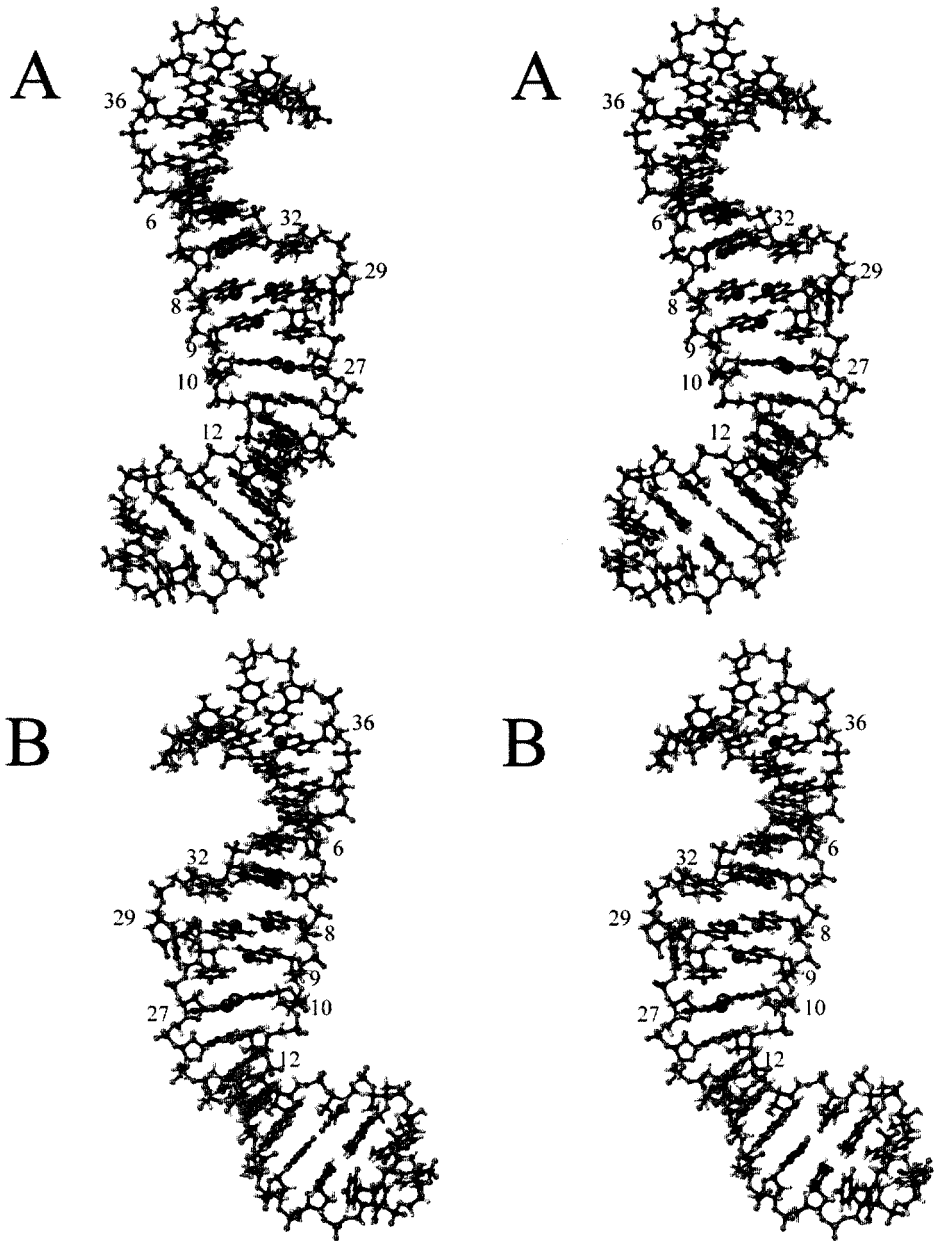

FIGURE 5: Stereoviews of ball-and-stick representations of the structure of domain B of the hairpin ribozyme with the N1 positions identified by the larger balls. Views of the internal loop major groove (A) and minor groove (B) are shown.

hairpin ribozyme (*4*). These adenine residues have apparent pK_a values of 6.5 and 6.2, respectively, and the protonated N1 group participates directly in a hydrogen bond. An apparent pK_a of 6.6 has been observed for A^+·C wobble base pairs in DNA oligonucleotide (*24*, *25*). However, the role of protonation in other types of adenine base pairs or in catalysis remains largely unexplored. A neutral apparent pK_a for an adenosine in the ribosomal peptidyl transferase center has very recently been reported, and a central role for this adenine in the catalytic mechanism was proposed (*5*).

The locations of the adenines in the three-dimensional structure of the B domain of the hairpin ribozyme are illustrated in Figure 5. The N1s of A8, A9, A10, A12, and A32 are in the minor groove while A6, A27, and A29 have their N1 exposed in the major groove. In addition to direct stabilization through hydrogen bonding discussed above for A^+·C base pairs, protonated adenines can also stabilize base pairs indirectly. Adenine amino protons become more acidic upon N1 protonation, enabling them to form stronger hydrogen bonds (*19*). The carbon−amino nitrogen bond gains additional double bond character upon N1 protonation, which results in restricted rotation that may also stabilize hydrogen-bonded amino groups (*26*). In the B domain internal loop, six of the eight adenines have hydrogen-bonded amino groups (A8, A9, A10, A12, A29, and A32).

If the protonated N1 is near a negatively charged phosphate, adenine protonation can lead to charge stabilization. In the internal loop of the B domain of the hairpin ribozyme, the A9, A10, A12, and A32 N1s are each 6−8 Å from phosphate groups on the opposite strand. Similar base pairings stabilized by protonated adenines have been observed in DNA (*8*, *27*). The A9, A10, A12, and A32 N1s are also all within 4 Å of 2′-oxygens on the opposite strand, as a result of their position in the minor groove, so it is possible that N1 protonation can result in hydrogen bond formation at these positions.

The A6·C33 (N1, amino) base pair has a geometry which is similar to that of a protonated A^+·C wobble, but the adenine N1 is nonprotonated and hydrogen bonded to the C33 amino group in the NMR structures calculated at pH 6.8 (Figure 2). The orientation of this base pair was somewhat surprising, because an A^+·C base pair has a similar geometry but forms an additional hydrogen bond, and a model had previously predicted the A6·C33 base pair to be a protonated A^+·C wobble pair (*28*). However, the data presented here show that A6 has a apparent pK_a value of 5.4, which is significantly lower than apparent pK_a values observed for A^+·C wobble pairs (*3*, *4*, *24*, *25*). The A6 apparent pK_a of 5.4 is higher than that of the mononucleotide or Watson−Crick-paired adenines (<3.1) (*2*), which suggests that the base pair is weak enough to still allow some degree of protonation. Alternatively, a pH-driven structural transition is possible, in which a small structural rearrangement (2−3 Å) could lead to the formation of a protonated wobble pair at low pH. A pH-driven structural equilibrium has been previously proposed for an A·C (N1, amino) base pair switching to an A^+·C wobble geometry at low pH, the former geometry being exactly the same as the A·C pair in the B domain (*24*).

The A12 and A32 of the B domain form A·G base pairs (Figure 2) and have raised apparent pK_as (Figure 4). The observed pK_a values are comparable to the value of 5.3 observed for adenine protonation in $d(A·G)_{10}$ (*27*). The Coulombic interactions between the protonated adenines and the backbone phosphate groups have been shown to result in increased stability of $d(A·G)_{10}$. Similar interactions can impart stability to the internal loop in the B domain. The A·G base pairs in the internal loop are in the type II A(anti)·G(anti) (*8*) orientation (Figure 2), which favors charge-stabilizing interactions.

Four adenines in the internal loop form A·A base pairs. Of these, A29 has the highest apparent pK_a of 5.8 while the other adenines (*9*, *10*, *27*) have relatively lower apparent pK_as of ∼4.9. In all cases, these are higher than the pK_a value of 3.5 for the mononucleotide. The lower apparent pK_a value of A9 and A10 may be partly due to the fact that the N1 functional group is close enough to form a hydrogen bond with the 2′-hydroxyl group of A29. Although the A9·A29 base pair is symmetrical, the N1 functional groups are in very different structural environments (Figure 5), accounting for the difference in their apparent pK_a values. The orientation of the A9·A29 base pair shown in Figure 2 is similar to the orientation of an A·A mispair observed in a DNA duplex (*8*). The pH titration curves reported for the adenines in the DNA duplex indicate an apparent pK_a value of about 5.5.

Stacking interactions play a large role in the B domain structure. Molecular orbital calculations have been carried out to study the effect of base protonation on intermolecular interactions (*29*). These calculations indicated that for all kinds of base pairs the magnitude of stacking interactions is increased upon protonation of one member of a stacking pair, although to differing extents. When both members of a stacking pair are protonated, stacking interactions become less favorable than for unprotonated pairs. Cross-strand stacking occurs between residues A8 and A32 (Figure 5). In this stacking pair, A32 is more readily protonated as indicated by its higher apparent pK_a value compared to A8. In the structure determination for domain B, a minor conformation was observed in which the pyrimidine residues C11, U26, and U28 are bulged out to allow stacking of the purine·purine base pairs (*14*). Such stacking would improve for a protonated A12 with an unprotonated A10 and for an unprotonated A27 with a protonated A29. The observed pK_as are higher for A12 and A29, which again correlates with one member of a purine·purine stacking pair being more readily protonated.

Proton Exchange in Adenines. Exchange of the proton at the N1 site in the protonated base can be described following the scheme used in imino proton exchange studies in Watson−Crick base pairs (*19*). The raised apparent pK_as (relative to the mononucleotide) observed for A6, A29, and A32 indicate that N1 protonation helps to stabilize the non-Watson−Crick base pairs involving these adenines. Proton exchange at the N1 site can be described as a two-step process.

$$A_{closed} \leftrightarrow A_{open} \leftrightarrow A(H^+)$$

In general, 'A_{closed}' refers to a state from which proton exchange cannot occur and is in equilibrium with the state 'A_{open}' from which proton exchange can occur. In the case of exchange in Watson−Crick base pairs, 'A_{closed}' refers to the base-paired configuration. From the solution structure determined for the B domain, the A6·C33 base pair has an orientation that may allow imino hydrogen bonding at low pH. The following imino exchange scheme would then be possible for the A6·C33 base pair:

$$A6·C33_{closed} \leftrightarrow A6\ C33_{open} \leftrightarrow A6(H^+)·C33$$

The other adenine base pairs may be involved in equilibria between two different orientations, one of which is feasible for proton exchange.

The first step in the above scheme is governed by conformational changes, and the second step is the exchange reaction. The most likely mechanism for the protonation and deprotonation of the adenine residues would be an acid/base-catalyzed reaction, with the rate depending on the concentration of the catalyst. The exchange rates would then be expected to show a pH dependence. The residues A6 and A32 show pH-dependent exchange rates, whereas A29 has exchange rates that are independent of pH (Table 2). The lack of pH dependence of the observed exchange rate of A29 implies that the rate-limiting step in the two-step exchange process at this site is a conformational change. Interestingly, A29 has an exposed N1 which would facilitate fast proton transfer, while the hydrogen bonds at its amino and N7 positions would make conformational changes of the A29·A9 base pair difficult. Even though A6 and A32 show a pH dependence for the exchange rates, the dependence is rather weak [plot of log(k_{obs}) versus pH has a slope of 0.5]. This indicates that the proton exchange reaction at the adenine N1 sites is faster than the conformational rearrangements of the base pairs.

CONCLUSIONS

The B domain of the hairpin ribozyme is one of the largest RNA structures solved by NMR to date, and is catalytically essential for the ribozyme. We have determined the apparent pK_a values of the adenines in the B domain of the hairpin

ribozyme, which contains an adenine-rich internal loop (16 nucleotides) with 8 adenines participating in 6 non-Watson−Crick base pairs. All of the adenines except the one involved in a Watson−Crick base pair were observed to have apparent pK_as significantly shifted with respect to that of the mononucleotide. The apparent pK_as for the adenines in the internal loop range from 4.8 to 5.8, significantly higher than the mononucleotide value of 3.5. The time scales of chemical exchanges associated with adenine protonation for several well-resolved adenines were found to be 10−50 μs. We conclude that the raised apparent pK_a values are likely to be the result of additional stabilizing interactions resulting from adenine protonation, including hydrogen bonds, stacking interactions, and charge stabilization. The observation that all of the adenine-containing non-Watson−Crick base pairs have raised apparent pK_a values suggests that this may be a general feature of adenine-rich RNA internal loops.

The observed pK_a values correlate remarkably well with the pH profiles of hairpin ribozyme reaction kinetics, which measure a shallow pH−rate profile with transitions centered at pH 5.4 and 9.8 (*13*). It is therefore possible that the ionization of an adenine functional group on the B domain may serve as the general acid catalyst responsible for the observed low pH transition, while the general base may be attributed to the loss of a hydrogen bond titrating at pH 9.8 (*13*). The direct participation of an adenine in the chemistry of the ribozyme would be consistent with the known metal ion independence of the mechanism. This study identifies two catalytically essential residues, A29 and A32, which have apparent pK_a values at or above pH 5.4. These adenines are therefore the most likely candidates for reaction chemistry (note that A29 and A32 in our B domain construct are actually A40 and A43, respectively, in the full ribozyme numbering scheme). However, domain docking may alter the apparent pK_a values observed here. In an attempt to identify exactly which adenine function may be involved in chemistry, we are currently in the process of investigating adenine protonation in the context of the full ribozyme.

REFERENCES

1. Fersht, A. (1985) *Enzyme structure and mechanism*, W. H. Freeman and Company, New York.
2. Saenger, W. (1984) *Principles of Nucleic Acid Structure*, Springer-Verlag, New York.
3. Legault, P., and Pardi, A. (1997) *J. Am. Chem. Soc. 119*, 6621−6628.
4. Cai, Z., and Tinoco, I., Jr. (1996) *Biochemistry 35*, 6026−6036.
5. Muth, G. W., Ortoleva-Donnelly, L., and Strobel, S. A. (2000) *Science 289*, 947−950.
6. Nissen, P., Hansen, J., Ban, N., Moore, P. B., and Steitz, T. A. (2000) *Science 289*, 920−930.
7. Nakano, S.-i., Chadalavada, D. M., and Bevilacqua, P. C. (2000) *Science 287*, 1493−1497.
8. Maskos, K., Gunn, B. M., LeBlanc, D. A., and Morden, K. M. (1993) *Biochemistry 32*, 3583−3595.
9. Gao, X., and Patel, D. J. (1988) *J. Am. Chem. Soc. 110*, 5178−5182.
10. Rajagopal, P., and Feigon, J. (1989) *Biochemistry 28*, 7859−7870.
11. Gehring, K., Leroy, J. L., and Gueron, M. (1993) *Nature 363*, 561−565.
12. McKay, D. B., and Wedekind, J. E. (1999) in *The RNA World, Second Edition* (Gesteland, R. F., Cech, T. R., and Atkins, J. F., Eds.) Cold Spring Harbor Laboratory Press, Cold Spring Harbor, NY.
13. Fedor, M. J. (2000) *J. Mol. Biol. 297*, 269−291.
14. Butcher, S. E., Allain, F. H.-T., and Feigon, J. (1999) *Nat. Struct. Biol. 6*, 212−216.
15. Butcher, S. E., Allain, F. H.-T., and Feigon, J. (2000) *Biochemistry 39*, 2174−2182.
16. Berzal-Herranz, A., Joseph, S., Chowrira, B. M., Butcher, S. E., and Burke, J. M. (1993) *EMBO J. 12*, 2567−2573.
17. Pinard, R., Lambert, D., Walter, N. G., Heckman, J. E., Major, F., and Burke, J. M. (1999) *J. Am. Chem. Soc. 38*, 16035−16039.
18. Kay, L. E., Keifer, P., and Saarinen, T. (1992) *J. Am. Chem. Soc. 114*, 10663−10665.
19. Guéron, M., and Leroy, J. L. (1995) *Methods Enzymol. 261*, 383−413.
20. Kay, L. E., Torchia, D. A., and Bax, A. (1989) *Biochemistry 28*, 8972−8979.
21. Bundi, A., and Wuthrich, K. (1979) *Biopolymers 18*, 285−297.
22. Gutowsky, H. S., and Holm, C. H. (1956) *J. Chem. Phys. 25*, 1228−1234.
23. Lane, A., and Lefevre, J.-F. (1994) *Methods Enzymol. 239*, 596−619.
24. Boulard, Y., Cognet, J. A. H., Gabarro-Arpa, J., LeBret, M., Sowers, L. C., and Fazakerley, G. V. (1992) *Nucleic Acids Res. 20*, 1933−1941.
25. Wang, C., Gao, H., Gaffney, B. L., and Jones, R. A. (1991) *J. Am. Chem. Soc. 113*, 5486−5488.
26. Shoup, R. R., Miles, H. T., and Becker, E. D. (1972) *J. Chem. Phys. 76*, 64−70.
27. Dolinnaya, N. G., and Fresco, J. R. (1992) *Proc. Natl. Acad. Sci. U.S.A. 89*, 9242−9246.
28. Earnshaw, D. J., Masquida, B., Muller, S., Sigurdsson, S. T., Eckstein, F., Westhof, E., and Gait, M. J. (1997) *J. Mol. Biol. 274*, 197−212.
29. Jordan, F., and Sostman, H. D. (1973) *J. Am. Chem. Soc. 95*, 6544−6554.

BI001976R